The 5 angstrom projection structure of the transmembrane domain of the mannitol transporter enzyme II

Koning, R.I; Keegstra, W.; Oostergetel, G.T.; Schuurman-Wolters, G.K.; Robillard, G.T.; Brisson, A.

Published in:
Journal of Molecular Biology

DOI:
10.1006/jmbi.1999.2650

Article No. jmbi.1999.2650 available online at http://www.idealibrary.com on IDEAL J. Mol. Biol. (1999) 287, 845–851

JMB

COMMUNICATION

The 5 Å Projection Structure of the Transmembrane Domain of the Mannitol Transporter Enzyme II

Roman I. Koning[1], Wilko Keegstra[1], Gert T. Oostergetel[1] Gea Schuurman-Wolters[2], George T. Robillard[2] and Alain Brisson[1]*

Departments of [1]Biophysical Chemistry and [2]Biochemistry Groningen Biomolecular Sciences and Biotechnology Institute, University of Groningen, Nijenborgh 4 9747, AG Groningen The Netherlands

**Corresponding author*

The uptake of mannitol in *Escherichia coli* is controlled by the phosphoenolpyruvate dependent phosphotransferase system. Enzyme II mannitol (EII^{Mtl}) is part of the phosphotransferase system and consists of three covalently bound domains. IIC^{Mtl}, the integral membrane domain of EII^{Mtl}, is responsible for mannitol transport across the cytoplasmic membrane. In order to understand this molecular process, two-dimensional crystals of IIC^{Mtl} were grown by reconstitution into lipid bilayers and their structure was investigated by cryo-electron crystallography. The IIC^{Mtl} crystals obey $p22_12_1$ symmetry and have a unit cell of 125 Å × 65 Å, $\gamma = 90°$. A projection structure was determined at 5 Å resolution using both electron images and electron diffractograms. The unit cell contains two IIC^{Mtl} dimers with a size of about 40 Å × 90 Å, which are oriented up and down in the crystal. Each monomer exhibits six domains of high density which most likely correspond to transmembrane α-helices and cytoplasmic loops.

Keywords: enzyme IIC mannitol; electron crystallography; 2-dimensional crystallisation; membrane protein; PTS

Substrate uptake in bacteria is mediated by different systems that either utilise concentration gradients across the membrane or accumulate the solute inside the cell at the expense of energy. The bacterial phosphoenolpyruvate (PEP)-dependent phosphotransferase system (PTS) catalyses the uptake of carbohydrates by a complex mechanism in which the phosphoryl group from PEP, which provides the energy for carbohydrate transport, is transferred to the carbohydrate *via* a series of soluble proteins and protein domains (Postma *et al.*, 1993). In addition to transport, PTS proteins are involved in chemotaxis (Lengeler & Vogler, 1989), regulation of carbohydrate metabolism (Saier & Reizer, 1994) and gene expression (Roseman & Meadow, 1990). The PTS consists of two general, non-sugar-specific and soluble proteins, enzyme I and HPr, and a sugar-specific membrane protein, known as enzyme II (EII; Lengeler *et al.*, 1994). EII is composed of three domains, two cytoplasmic and one membrane-bound, which may be linked in different ways, depending on the sugar-specificity. In the mannitol-specific EII (EII^{Mtl}) of *Escherichia coli*, the three domains are covalently associated (Saier *et al.*, 1988). The IIA^{Mtl} cytoplasmic domain accepts the phosphoryl from HPr and transfers it to the IIB^{Mtl} cytoplasmic domain which transfers it to the mannitol. The integral membrane domain IIC^{Mtl} is responsible for mannitol translocation across the cytoplasmic membrane. The EII^{Mtl} has been proposed to exist as a dimer, both in the cytoplasmic membrane and in detergent-solubilised form (Pas *et al.*, 1987; Khandekar & Jacobson, 1989). The fact that mannitol fermentation could be restored by co-expressing two different inactive mutants provided direct evidence for EII^{Mtl} dimer formation both *in vitro* and *in vivo* (Boer *et al.*, 1996). It has been proposed that this dimerisation is mediated *via* non-covalent hydrophobic inter-

Abbreviations used: 2-D, two-dimensional; PEP, phosphoenolpyruvate; PTS, phosphotransferase system; EII^{Mtl}, enzyme II mannitol; IIC^{Mtl}, integral membrane domain of EII^{Mtl}; DOPC, dioleoyl phosphatidylcholine; egg-PC, egg phosphatidylcholine; DOPE, dioleoyl phosphatidylethanolamine; CHAPS, 3-[(3-cholamidopropyl)dimethylammonio]-1-propanesulfonate; CHAPSO, 3-[(3-cholamidopropyl)dimethylammonio]-2-hydroxy-1-propanesulfonate.

E-mail address of the corresponding author: brisson@chem.rug.nl

0022-2836/99/150845–07 $30.00/0

actions at the level of the C-domains (Lolkema *et al.*, 1993).

In recent years the structure of several cytoplasmic PTS proteins and domains from several bacterial sources have been solved by X-ray crystallography or NMR spectroscopy. The structures of HPr (Jia *et al.*, 1993), the N-terminal half of enzyme I (Liao *et al.*, 1996), IIA^{Mtl} (van Montfort *et al.*, 1998), IIA^{Man} (Nunn *et al.*, 1996), IIA^{Glc} (Worthylake *et al.*, 1991) IIB^{Cel} (van Montfort *et al.*, 1997) and IIB^{Glc} (Eberstadt *et al.*, 1996) from *E. coli*, IIA^{Glc} (Liao *et al.*, 1991), IIB^{Lev} (Schauder *et al.*, 1998) from *Bacillus subtilus*, and IIA^{Lac} (Sliz *et al.*, 1997) from *Lactobacillus lactis* are known at atomic resolution. On the other hand, structural information on the integral membrane domain of EII, which is responsible for sugar transport, is yet very limited. Secondary structure predictions based on an hydrophobicity analysis proposed that IIC^{Mtl} presents seven α-helical stretches and two large hydrophilic cytoplasmic loops (Lee & Saier, 1983). On the other hand, results from *PhoA-mtlA* gene fusion techniques led to a model consisting of only six membrane-spanning α-helices, together with two large cytoplasmic loops (Sugiyama *et al.*, 1991). This latter topology agrees with the ''posi-

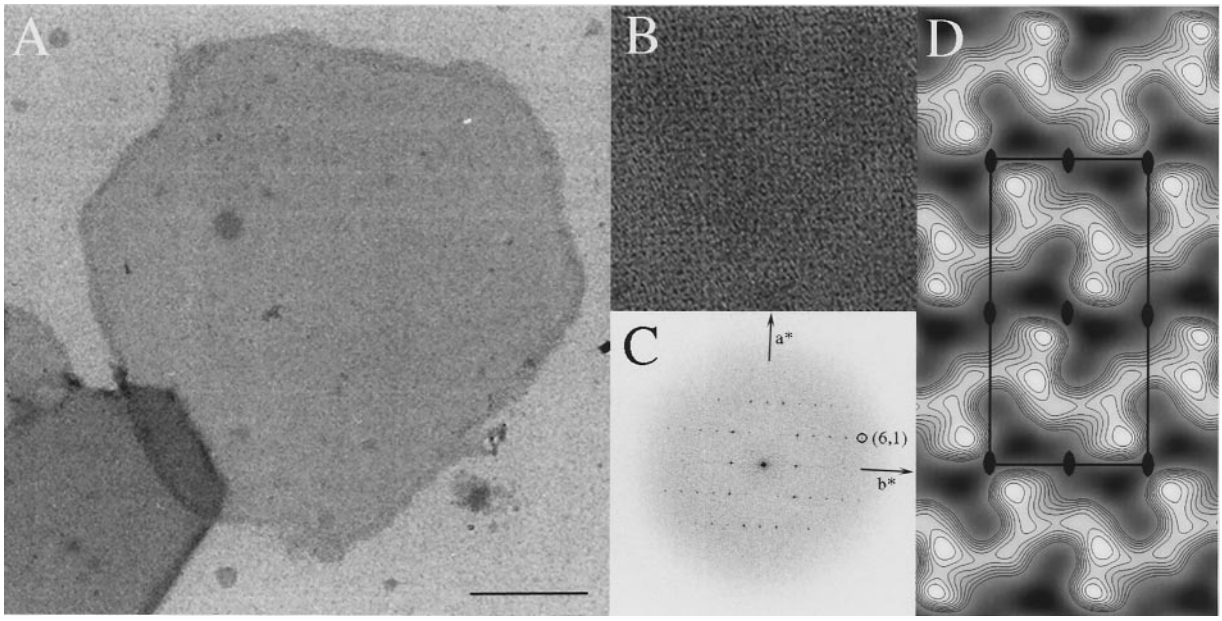

Figure 1. (a) and (b) Typical electron micrographs of negatively stained 2-D crystals of IIC^{Mtl} (scale bar in (a) represents 500 nm; image size (b) represents 125 nm × 125 nm). (c) Fourier transform of a negatively stained crystal of IIC^{Mtl} is shown with the (6,1) reflection at 20 Å circled and the a^* and b^* lattice vectors indicated. (d) The 2-D projection map of negatively stained IIC^{Mtl} crystals at 20 Å resolution. One unit cell and the $p2$ symmetry elements are outlined. This map was calculated after merging four images and imposing $p2$ symmetry. Protein densities are represented with eight contour levels, equally spaced from mean to highest density. In this projection map, two types of dimers of IIC^{Mtl} are visible (one located at the edges of the unit cell, the other one located at its centre). These two types of dimers have an overall similar shape, yet a slightly differing density distribution, which is likely to be due to uneven staining between the two sides of a crystal. Methods: *E. coli* IIC^{Mtl}, presenting a C-terminal His_6-tag was grown in *E. coli* and extracted from membrane vesicles with a buffer containing 0.5 % (w/v) sodium deoxycholate, 20 mM Tris (pH 8.4), 300 mM NaCl, 3 mM NaN_3 and 2 mM β-mercaptoethanol and purified by affinity chromatography with Ni-agarose (Quiagen) in the presence of 20 mM imidazole, as described earlier (Meijberg *et al.*, 1998). IIC^{Mtl}, bound to the Ni-column was washed with a buffer containing 6 mM decylmaltoside, 20 mM Tris (pH 7.5), 150 mM NaCl, 20 mM imidazole, 3 mM NaN_3 and 2 mM β-mercaptoethanol and was eluted in the presence of 200 mM imidazole providing a pure protein solution as observed by silver-stained SDS-PAGE. The IIC^{Mtl} concentration (typically 0.7 - 1.4 mg/ml) was determined using a calculated molar extinction coefficiënt $\varepsilon_{280} = 31{,}190/M \times cm$ (Pace *et al.*, 1995). Solubilised IIC^{Mtl} was supplemented with a solution of 2.0 mg/ml *E.coli* lipid extract, which was repurified by aceton/ether extraction, solubilised in 20 mg/ml CHAPS. Detergent was dialysed against a buffer containing 25 mM Hepes (pH 7.5), 150 mM NaCl, 5 mM EDTA, 3 mM NaN_3, 2 mM β-mercaptoethanol and 1 mM mannitol at 4°C. Crystallisation experiments were performed in glass capilary tubes (1.5 mm × 35 mm) at a lipid to protein ratio close to 1.0 (w/w) using dialysis membranes with a M_r cut-off of 12-14 kDa (Spectra/Por). Buffer was renewed several times during dialysis. For cryo-electron microscopy, 200 mesh molybdenum grids (Okenshoji Co. Ltd) coated with a thin carbon layer were used (Brisson *et al.*, 1999). Carbon films were checked for planarity before use with a reflected light microscope (Schmutz & Brisson, 1996). Only planar grids without defects were selected for further use. Crystals were transferred onto the grids after glow discharging the grids in air. Specimens were rapidly frozen into liquid ethane using a modified KF80 cryo-system (Reichert-Jung) and were mounted in a Gatan type 626 cryo-specimen holder. For negative staining, 400 mesh copper grids (Agar Scientific) coated with a formvar-carbon layer were used and specimens were stained with a 1 % (w/v) uranylacetate solution (pH 3.5).

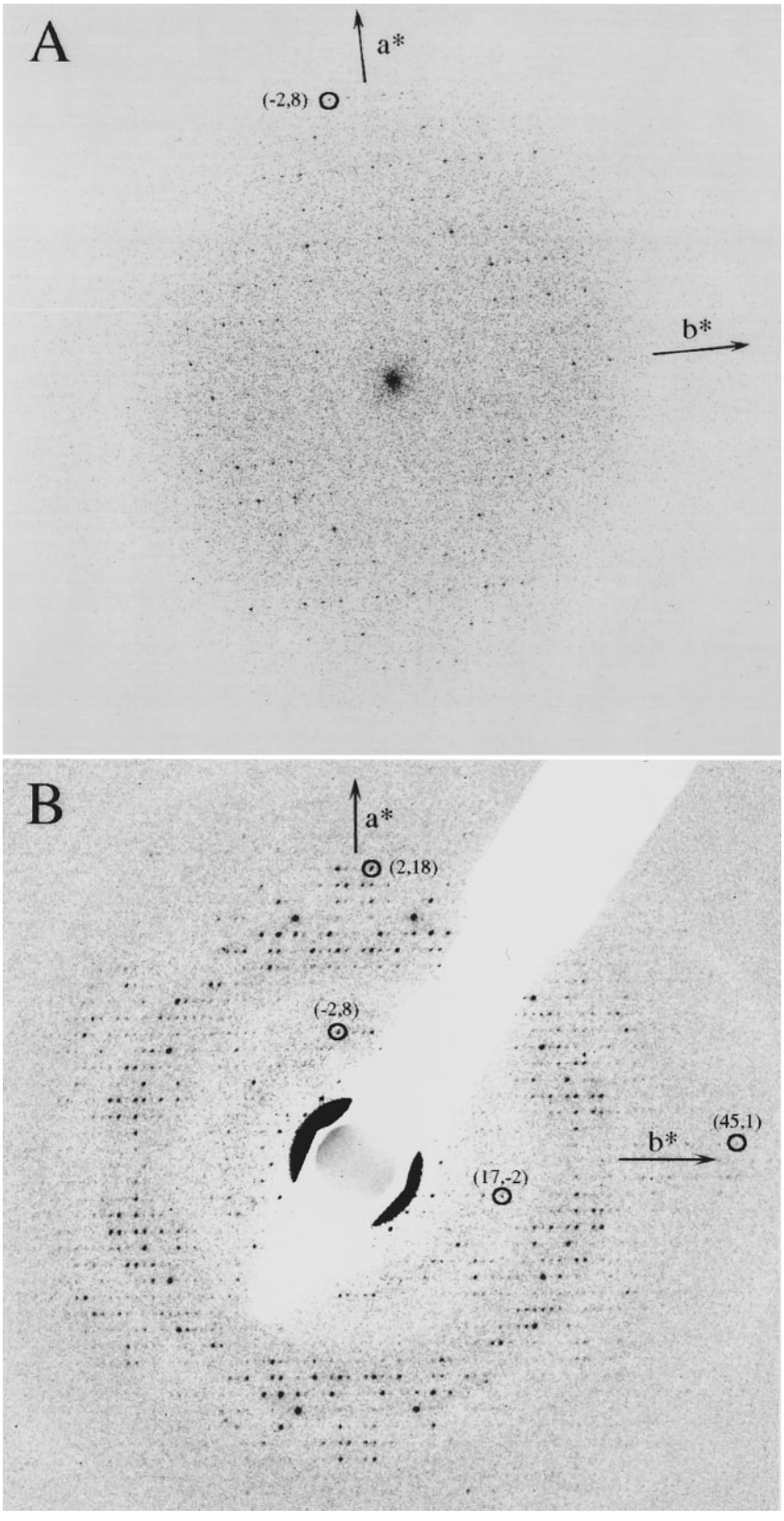

Figure 2. (a) Fourier transform of an electron image of a frozen-hydrated IIC^{Mtl} crystal. The a^* and b^* lattice vectors are indicated. The (−2,8) reflection at 8.0 Å resolution is circled. (b) Background-subtracted electron diffractogram of a frozen-hydrated IIC^{Mtl} crystal. The (2,18) reflection at 3.6 Å and the (45,1) reflections at 2.7 Å are circled, together with the (−2,8) reflection also indicated in (a). Methods: Cryo-electron images were recorded using a Philips CM200-FEG equipped with a 14 bit 1000 × 1000 Gatan type 794 Multi-Scan CCD, operated at 200 kV. Selection of potentially good crystals was performed using an automated system of data acquisition recently developed (Oostergetel *et al.*, 1998). Micrographs were recorded at a magnification of 66,000× and at 75-400 nm underfocus on AGFA scientia EM films. Films were developed for 12 minutes in full-strength Kodak D-19 developer. Electron diffractograms were recorded with the CCD-camera at an accelerating voltage of 200 kV, a camera length of 880 mm and a 30 μm condensor aperture. A beam stop was used to prevent damage to the camera, and a selected area aperture, corresponding to a 1 μm size at the specimen level, was used to suppress satellite spots generated by the FEG tip in diffraction mode. An exposure time of 15 to 40 seconds was used, with an electron dose of about 1-4 e/Å^2.

tive inside rule'', a well-established empirical rule based on a diferrence in charge distribution between translocated and non-translocated loops (von Heijne, 1992), and is also consistent with trypthophan fluorescence studies (Dijkstra *et al.*, 1996). Although the hydrophobicity plots of EII^{Mtl} and EII^{Glc} are very similar, a topological model consisting of eight transmembrane α-helices has been predicted for the related EII^{Glc} on the basis of the *PhoA* fusion technique (Buhr & Erni, 1993).

Table 1. Image statistics of IIC^{Mtl}

Two-sided plane group		$p22_12_1$
Cell parameters ($n = 7$)		$a = 124.8(\pm0.8)$ Å $b = 64.7(\pm0.5)$ Å $\gamma = 90.1(\pm0.3)^\circ$
Electron diffraction		
Number of electron diffraction images		2
Number of observations		1091
Electron images		
Number of merged images		4
Total number of unique reflections (to 5 Å, IQ 6)		439
Total number of observations (4 images, to 5 Å, IQ 6)		909
Mean phase residual (to 5 Å, IQ 6) (deg.)		27.9
Phase residual in resolution ranges (IQ 6)		
Resolution range (Å)	Phase residual (°)	Completeness (%)
100.00-5.00	27.9	88
100.00-14.14	15.3	100
14.13-10.00	11.0	100
9.99-8.16	13.3	100
8.15-7.07	29.7	97
7.06-6.32	36.5	85
6.31-5.77	31.6	86
5.76-5.35	42.8	79
5.34-5.00	52.5	76

To delineate the structural features that are responsible for selective sugar transport, it is necessary to determine the structure of a IIC domain at high resolution in a lipid bilayer. We present here the projection structure of IIC^{Mtl} at 5 Å resolution, calculated by electron crystallography (Henderson *et al.*, 1990) of frozen-hydrated 2-D crystals.

Two-dimensional crystallisation of IIC^{Mtl}

IIC^{Mtl}, expressed with a poly-histidine extension, was crystallised in 2-D by reconstitution into lipid bilayers after detergent dialysis. Crystal formation started with the formation of liposomes, which were growing like a bunch of grapes from a central aggregate. After two weeks of extensive detergent dialysis, sheet-like crystals emerged from these aggregates, measuring 1 to 5 μm (Figure 1(a) and (b)). The 2-D crystals of IIC^{Mtl} embedded in negative stain diffracted up to 20 Å (Figure 1(c)). The nature of both lipids and detergents was the most important parameter in crystal formation. IIC^{Mtl} crystals were obtained using *E. coli* lipid extracts, which consist of phosphatidylethanolamine, phosphatidylglycerol and cardiolipin, and also, but to a lesser extent, with either DOPC, egg-PC or DOPE. Amongst the following detergents: $C_{12}E_8$, $C_{12}E_9$, octylglucoside, dodecylmaltoside, CHAPSO, Triton X-100, decylmaltoside and CHAPS, only decylmaltoside and CHAPS induced crystal formation. Using a mixture of both CHAPS and decylmaltoside during dialysis improved both crystal quality and quantity. Crystal formation was almost independent of the lipid to protein ratio within a range of 0.5 to 1.5 (w/w). More crystals were obtained when EDTA was added to the dialysis buffer, which reduced the aggregation observed in the presence of the divalent cations Ca^{2+}, Mg^{2+} and Ni^{2+}.

The IIC^{Mtl} crystals presented a tendency to form multilayers, as it is obvious from the thick edges and the different grey levels of the crystals shown in Figure 1(a). For the structural analysis presented below, we focused on the thinnest crystals. The fact that only one type of projection structure was consistently observed indicates either that these crystals were single-layered or consisted of thin multi-layers stacked in register. This aspect will be carefully considered in the analysis of their three-dimensional structure.

Frozen-hydrated 2-D crystals of IIC^{Mtl} were highly ordered, diffracting electrons up to 2.7 Å (Figure 2(b)). Images of frozen-hydrated IIC^{Mtl} crystals reproducibly showed diffraction peaks extending up to 7 Å, while peaks were visible by optical diffraction at 4.6 Å in four images (Figure 2(a)). The unit cell dimensions are $a = 124.8$ (±0.8) Å, $b = 64.7$ (±0.5) Å and $\gamma = 90.1$ (±0.3)° ($n = 7$) (Table 1). Fourier transforms of individual images showed a strongly marked mm symmetry and a systematic absence of diffraction peaks with odd indices along the reciprocal axes. After origin refinement, the phases of the structure factors are near 0 or π, and satisfy the characteristic $p22_12_1$ phase relationship $\phi(h, k) = (h + k)\pi + \phi(h, -k)$.

Projected structure of IIC^{Mtl}

The 2-D projection maps calculated at 7 Å resolution from individual electron images of frozen-hydrated IIC^{Mtl} crystals showed a marked $p22_12_1$ symmetry (Figure 3(a)). In contrast to frozen-hydrated crystals, negatively stained crystals did not obey $p22_12_1$ but $p2$ symmetry (Figure 1(d)), which is most probably due to an uneven staining of both sides of the crystals. A 5 Å projection map was calculated by combining data from two electron diffraction patterns and four images (Figure 3(b)). The IIC^{Mtl} crystal is composed of

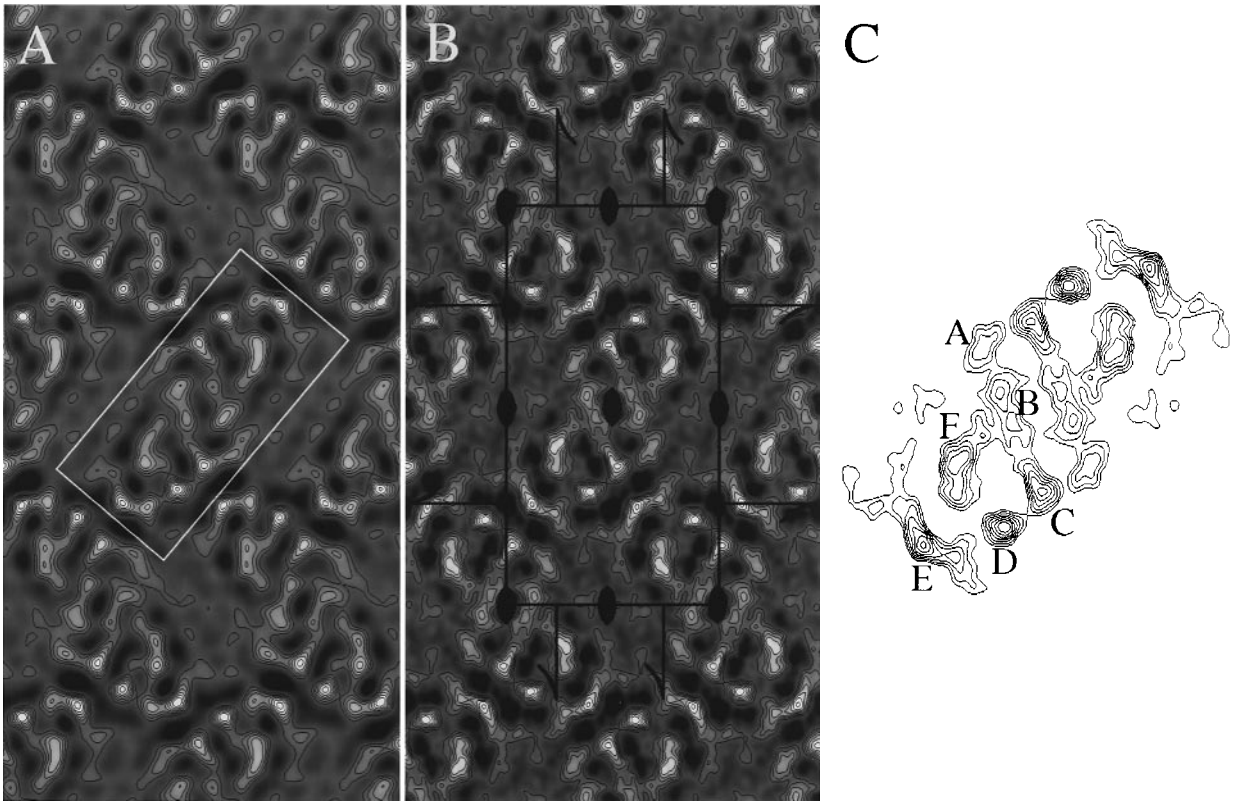

Figure 3. (a) 2-D projection map at 7.0 Å resolution of one electron image of a frozen-hydrated IIC^{Mtl} crystal, without any symmetry imposed. One IIC^{Mtl} dimer is enclosed within a white box. (b) 2-D projection structure of IIC^{Mtl} at 5 Å resolution, calculated by merging the data from two electron diffractograms and four electron images of frozen-hydrated IIC^{Mtl} crystals. One unit cell and the $p22_12_1$ symmetry elements are shown. (c) Structure of a IIC^{Mtl} dimer. In one monomer, the six main protein densities are labelled A to F. Methods: For determination of the structure factors the best micrographs were selected by optical diffraction and digitized with a Leafscan 45 CCD-array microdensitometer with a 10 μm step size, corresponding to 1.5 Å at the specimen level. Areas ranging up to 3584 × 3584 pixels in size, corresponding to 0.54 μm × 0.54 μm at the specimen level were processed. Image processing was performed by combining the MRC suite of programs (Crowther *et al.*, 1996) and a newly developed image processing package (W.K. & A.B., unpublished data), as follows: (i) for each individual image, phases were corrected for (CTF) effects and unbending was applied to correct for lattice distortions; (ii) four images were merged in $p1$ using the best image as a reference; (iii) $p22_12_1$ symmetry was imposed to the merged data set. Electron diffraction patterns were processed by the MRC suite of programs (Baldwin & Henderson, 1984) as follows: (i) the radial background distribution was calculated and subtracted from the image; (ii) the intensities from two electron diffraction patterns were scaled using diffraction peaks present in both data sets and merged. Finally, the amplitudes calculated from the merged electron diffraction data set were scaled with those from the merged image data set, using peaks present in both data sets, and combined with the phases to calculate the final map.

oval motifs of about 90 Å × 40 Å (Figure 3(a), white box), which lie in alternating rows, in up and down orientations. Each oval motif presents a 2-fold symmetry axis, perpendicular to the crystal plane, located at its centre and must therefore correspond to a dimer of IIC^{Mtl}. This is supported by the fact that the primary sequence of IIC^{Mtl} shows no internal homology, and by comparison of the projected sizes of IIC^{Mtl} and bacteriorhodopsin (Unwin & Henderson, 1975) taking into account the molecular weight difference. The two IIC^{Mtl} molecules within each dimer have the same up or down orientation, and might therefore represent the biologically active dimer.

Although the IIC^{Mtl} dimers are well resolved within the crystal, the molecular boundary of the monomers within a dimer is not apparent. We tentatively propose that one monomer is formed by six domains of high protein density, labelled A to F in Figure 3(c), and that monomers interact *via* a straight interface, although the attribution of domain A to one or the other monomer is still ambiguous. Adjacent domains are separated by 10 to 20 Å and all are around 8 Å wide. They have comparable shapes to the densities observed in projection maps of bacteriorhodopsin and therefore we postulate that most of these domains are transmembrane α-helices. Domains C and D are the most compact and are likely to represent α-helices oriented almost perpendicular to the membrane. Domains B and F are more elongated and of lower density and therefore are proposed to be α-helices more or less tilted with respect to the membrane. Domain E has a curved shape and seems too large

for a single transmembrane α-helix. It could either correspond to two overlapping helices or to one helix associated with an extramembrane domain, such as one of the two postulated large cytoplasmic loops. By comparison with the other domains, the density of domain A seems small for a transmembrane α-helix. If we combine this structural information with the topological models already proposed for IIC^{Mtl} (Lee & Saier, 1983; Sugiyama *et al*., 1991) it is likely that the transmembrane portion of IIC^{Mtl} consists of six α-helices.

Two low-density regions were consistently resolved in all processed images, consisting either of the region enclosed by helices B, C, D and F, or of the extended region forming the monomer-monomer interface. Although the available data do not allow us to speculate about the possible involvement of either one of these regions as a mannitol pathway, it is worth mentioning the hypothesis that two IIC^{Mtl} monomers form a common binding site and/or translocation pathway upon dimerisation (Saraceni-Richards & Jacobson, 1997). A three-dimensional analysis at high resolution of IIC^{Mtl} structure is required to determine its exact secondary structure and to provide futher information about the mechanism of sugar transport.

Acknowledgements

We thank Egbert Boekema for fruitful discussions and Olivier Lambert for help in scanning the micrographs. We acknowledge the contribution of Guy Perkins and Wilma Bergsma-Schutter at early stages of this project. This work was supported by the EU (grant BIO4 CT96-0129 to A.B.). R.I.K. is a recipient of a SON PhD fellowship.

References

Baldwin, J. M. & Henderson, R. (1984). Measurement and evaluation of electron diffraction patterns from two-dimensional crystals. *Ultramicroscopy,* **14**, 319-336.

Boer, H., ten Hoeve-Duurkens, R. H. & Robillard, G. T. (1996). Relation between the oligomerization state and the transport and phosphorylation function of the *Escherichia coli* mannitol transport protein: interaction between mannitol-specific enzyme II monomers studied by complementation of inactive site-directed mutants. *Biochemistry,* **35**, 12901-12908.

Brisson, A., Lambert, O. & Bergsma-Schutter, W. (1999). *Crystallization of Nucleic Acids and Proteins: A Practical Approach* (Ducruix, A. & Giegé, R., eds), in the press, Oxford University Press, Oxford.

Buhr, A. & Erni, B. (1993). Membrane topology of the glucose transporter of *Escherichia coli*. *J. Biol. Chem.* **268**, 11599-11603.

Crowther, R. A., Henderson, R. & Smith, J. M. (1996). MRC image processing programs. *J. Struct. Biol.* **116**, 9-16.9.

Dijkstra, D. S., Broos, J., Lolkema, J. S., Enequist, H., Minke, W. & Robillard, G. T. (1996). A fluorescence study of single tryptophan-containing mutants of enzyme IImtl of the *Escherichia coli* phosphoenolpyruvate-dependent mannitol transport system. *Biochemistry,* **35**, 6628-6634.

Eberstadt, M., Grdadolnik, S. G., Gemmecker, G., Kessler, H., Buhr, A. & Erni, B. (1996). Solution structure of the IIB domain of the glucose transporter of *Escherichia coli*. *Biochemistry,* **35**, 11286-11292.

Henderson, R., Baldwin, J. M., Ceska, T. A., Zemlin, F., Beckmann, E. & Downing, K. H. (1990). Model for the structure of bacteriorhodopsin based on high-resolution electron cryo-microscopy. *J. Mol. Biol.* **213**, 899-929.

Jia, Z., Quail, J. W., Waygood, E. B. & Delbaere, L. T. (1993). The 2.0 Å resolution structure of *Escherichia coli* histidine-containing phosphocarrier protein HPr. A redetermination. *J. Biol. Chem.* **268**, 22490-22501.

Khandekar, S. S. & Jacobson, G. R. (1989). Evidence for two distinct conformations of the *Escherichia coli* mannitol permease that are important for its transport and phosphorylation functions. *J. Cell Biochem.* **39**, 207-216.

Lee, C. A. & Saier, M. H., Jr (1983). Mannitol-specific enzyme II of the bacterial phosphotransferase system. III. The nucleotide sequence of the permease gene. *J. Biol. Chem.* **258**, 10761-10767.

Lengeler, J. W. & Vogler, A. P. (1989). Molecular mechanisms of bacterial chemotaxis towards PTS-carbohydrates. *FEMS Microbiol. Rev.* **5**, 81-92.

Lengeler, J. W., Jahreis, K. & Wehmeier, U. F. (1994). Enzymes II of the phospho-enolpyruvate-dependent phosphotransferase systems: their structure and function in carbohydrate transport. *Biochim. Biophys. Acta,* **1188**, 1-28.

Liao, D. I., Kapadia, G., Reddy, P., Saier, M. H., Jr, Reizer, J. & Herzberg, O. (1991). Structure of the IIA domain of the glucose permease of *Bacillus subtilis* at 2.2 Å resolution. *Biochemistry,* **30**, 9583-9594.

Liao, D. I., Silverton, E., Seok, Y. J., Lee, B. R., Peterkofsky, A. & Davies, D. R. (1996). The first step in sugar transport: crystal structure of the amino terminal domain of enzyme I of the *Escherichia coli* PEP: sugar phosphotransferase system and a model of the phosphotransfer complex with HPr. *Structure,* **4**, 861-872.

Lolkema, J. S., Kuiper, H., ten Hoeve-Duurkens, R. H. & Robillard, G. T. (1993). Mannitol-specific enzyme II of the phosphoenolpyruvate-dependent phosphotransferase system of *Escherichia coli*: physical size of enzyme II^{Mtl} and its domains IIBA and IIC in the active state. *Biochemistry,* **32**, 1396-1400.

Meijberg, W., Schuurman-Wolters, G. K., Boer, H., Scheek, R. M. & Robillard, G. T. (1998). The thermal stability and domain interactions of the mannitol permease of *Escherichia coli*. A differential scanning calorimetry study. *J. Biol. Chem.* **273**, 20785-20794.

Newman, M. J. & Wilson, T. H. (1980). Solubilization and reconstitution of the lactose transport system from *Escherichia coli*. *J. Biol. Chem.* **255**, 10583-10586.

Nunn, R. S., Markovic-Housley, Z., Genovesio-Taverne, J. C., Flukiger, K., Rizkallah, P. J., Jansonius, J. N., Schirmer, T. & Erni, B. (1996). Structure of the IIA domain of the mannose transporter from *Escherichia coli* at 1.7 Å resolution. *J. Mol. Biol.* **259**, 502-511.

Oostergetel, G. T., Keegstra, W. & Brisson, A. (1998). Automation of specimen selection and data acquisition for protein electron crystallography. *Ultramicroscopy,* **74**, 47-32.

Pace, C. N., Vajdos, F., Fee, L., Grimsley, G. & Gray, T. (1995). How to measure and predict the molar absorption coefficient of a protein. *Protein Sci.* **4**, 2411-2423.

Pas, H. H., Ellory, J. C. & Robillard, G. T. (1987). Bacterial phosphoenolpyruvate-dependent phosphotransferase system: association state of membrane-bound mannitol-specific enzyme II demonstrated by inactivation. *Biochemistry*, **26**, 6689-6696.

Postma, P. W., Lengeler, J. W. & Jacobson, G. R. (1993). Phosphoenolpyruvate carbohydrate phosphotransferase systems of bacteria. *Microbiol. Rev.* **57**, 543-594.

Roseman, S. & Meadow, N. D. (1990). Signal transduction by the bacterial phosphotransferase system. Diauxie and the crr gene. *J. Biol. Chem.* **265**, 2993-2996.

Saier, M. H., Jr & Reizer, J. (1994). The bacterial phosphotransferase system: new frontiers 30 years later. *Mol. Microbiol.* **13**, 755-764.

Saier, M. H., Jr, Yamada, M., Erni, B., Suda, K., Lengeler, J. W., Ebner, R., Argos, P., Rak, B., Schnetz, K. & Lee, C. A. (1988). Sugar permeases of the bacterial phosphoenolpyruvate-dependent phosphotransferase system: sequence comparisons. *FASEB J.* **2,** 199-208.

Saraceni-Richards, C. A. & Jacobson, G. R. (1997). Subunit and amino acid interactions in the *Escherichia coli* mannitol permease: a functional complementation study of coexpressed mutant permease proteins. *J. Bacteriol.* **179**, 5171-5177.

Schauder, S., Nunn, R. S., Lanz, R., Erni, B. & Schirmer, T. (1998). Crystal structure of the IIB subunit of a fructose permease (IIBLev) from *Bacillus subtilis*. *J. Mol. Biol.* **276**, 591-602.

Schmutz, M. & Brisson, A. (1996). Analysis of carbon film planarity by reflection light microscopy. *Ultramicroscopy*, **63**, 263-272.

Sliz, P., Engelmann, R., Hengstenberg, W. & Pai, E. F. (1997). The structure of enzyme IIA lactose from *Lactococcus lactis* reveals a new fold and points to possible interactions of a multicomponent system. *Structure,* **5**, 775-788.

Sugiyama, J. E., Mahmoodian, S. & Jacobson, G. R. (1991). Membrane topology analysis of *Escherichia coli* mannitol permease by using a nested-deletion method to create mtlA-phoA fusions. *Proc. Natl Acad. Sci. USA,* **88**, 9603-9607.

Unwin, P. N. T. & Henderson, R. (1975). Molecular structure determination by electron microscopy of unstained crystalline specimens. *J. Mol. Biol.* **94**, 425-440.

van Montfort, R. L. M., Pijning, T., Kalk, K. H., Reizer, J., Saier, M. H., Jr, Thunnissen, M. M., Robillard, G. T. & Dijkstra, B. W. (1997). The structure of an energy-coupling protein from bacteria, IIB cellobiose, reveals similarity to eukaryotic protein tyrosine phosphatases. *Structure,* **5**, 217-225.

van Montfort, R. L. M., Pijning, T., Kalk, K. H., Hangyi, I., Kouwijzer, M. L., Robillard, G. T. & Dijkstra, B. W. (1998). The structure of the *Escherichia coli* phosphotransferase IIA mannitol reveals a novel fold with two conformations of the active site. *Structure,* **6**, 377-388.

von Heijne, G. (1992). Membrane protein structure prediction. Hydrophobicity analysis and the positive-inside rule. *J. Mol. Biol.* **225**, 487-494.

Worthylake, D., Meadow, N. D., Roseman, S., Liao, D. I., Herzberg, O. & Remington, S. J. (1991). Three-dimensional structure of the *Escherichia coli* phosphocarrier protein IIIglc. *Proc. Natl Acad. Sci. USA,* **88**, 10382-10386.

Edited by W. Baumeister

(Received 16 November 1998; received in revised form 18 February 1999; accepted 18 February 1999)